Applied Catalysis B: Environment and Energy 349 (2024) 123842

Contents lists available at ScienceDirect

Applied Catalysis B: Environment and Energy

journal homepage: www.elsevier.com/locate/apcatb

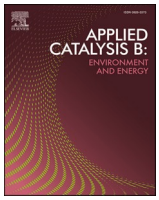

Tailoring the product distribution of CO_2 hydrogenation via engineering of Al location in zeolite

Yongqiang Gu [a,b,1], Jie Liang [c,1], Yang Wang [a,b,*], Kaixuan Huo [a], Meng Li [a], Wenhang Wang [b], Ruosong He [a], Shuhei Yasuda [b], Xinhua Gao [c], Guohui Yang [b], Mingbo Wu [a], Noritatsu Tsubaki [b,**]

[a] College of New Energy, State Key Laboratory of Heavy Oil Processing, China University of Petroleum (East China), Qingdao 266580, China
[b] Department of Applied Chemistry, Graduate School of Engineering, University of Toyama, Gofuku 3190, Toyama 930-8555, Japan
[c] State Key Laboratory of High-efficiency Utilization of Coal and Green Chemical Engineering, College of Chemistry & Chemical Engineering, Ningxia University, Yinchuan 750021, China

ARTICLE INFO

Keywords:
CO_2 conversion
Al location
Acid property
Product distribution

ABSTRACT

Even though tremendous progress has been made on modified Fischer-Tropsch synthesis (FTS) multifunctional catalyst that composed of Fe-based component and acidic zeolite H-ZSM-5 for CO_2 hydrogenation into value-added chemicals, the structure-function relationship between the acidic zeolite H-ZSM-5 and product distribution is still under debate. Herein, a series of H-ZSM-5 zeolites with different Al locations and acidic properties are fabricated by varying the synthesis raw agents and conditions. After combining with the carbon-encapsulated Fe-based catalyst for alkenes synthesis from CO_2 hydrogenation, aromatics are directionally produced from the ellipsoidal H-ZSM-5 with Al species mainly located at the intersection of straight and sinusoidal channels, while the main products shift to iso-paraffins for the H-ZSM-5 with pillared nanosheet morphology owing to its Brønsted acid site-rich property. The Al location in H-ZSM-5 and the corresponding acidic property are systematically investigated, and the theoretical simulations illustrate that the Al species at the intersection channels could lower the energy barrier of key aromatization step. The Al richly located at straight/sinusoidal would boost the isomerization reaction. Our work not only clarifies the structure-function relationship of acidic zeolite H-ZSM-5 in valuable chemicals synthesis from CO_2 hydrogenation but also provides a novel protocol for controlled synthesis.

1. Introduction

The increasing CO_2 emissions, along with the development of human society, have caused numerous environmental issues, including global warming, climate change, ocean acidification, etc [1,2]. CO_2 is not only a major component of greenhouse gases but also an abundant, cheap, and non-toxic C1 resource. Therefore, the transformation of CO_2 into value-added chemicals could effectively mitigate the environmental troubles of CO_2 emissions [3–6].

Thermal-catalytic hydrogenation technology for CO_2 transformation has attracted wide attention due to its high efficiency and industrial applicability [7–11]. Recently, the tandem catalysis strategy that coupling several reactions in a one-step for CO_2 conversion into C2+ products, e.g., liquid fuels and aromatics, has made the thermal-catalytic CO_2 hydrogenation technology more promising [12–15]. For instance, Sun et al. developed a physically mixing bifunctional catalyst that composed of reducible metal oxide In_2O_3 and acidic zeolite H-ZSM-5 to realize the direct conversion of CO_2+H_2 into liquid fuels dominated by iso-paraffins via the methanol-mediated pathway [12]. Interestingly, the main product was shifted to aromatics by employing a series of bifunctional catalysts, such as Cr_2O_3/H-ZSM-5, ZnZrO/ZSM-5, ZnAlOx&H-ZSM-5, etc., which can be attributed to the unique acidic property of H-ZSM-5 zeolite [13–15]. However, for the methanol-mediated pathway, the high reaction temperature that needed by methanol

* Corresponding author at: College of New Energy, State Key Laboratory of Heavy Oil Processing, China University of Petroleum (East China), Qingdao 266580, China.
** Corresponding author.
E-mail addresses: wangyang@upc.edu.cn (Y. Wang), tsubaki@eng.u-toyama.ac.jp (N. Tsubaki).
[1] Co-first author

https://doi.org/10.1016/j.apcatb.2024.123842
Received 10 December 2023; Received in revised form 6 February 2024; Accepted 12 February 2024
Available online 24 February 2024

conversion on acidic zeolite usually leads to high CO selectivity from the reducible metal oxide-catalyzed methanol synthesis process, therefore lowering the yield of the targeted product. In addition to the methanol-mediated pathway, the multifunctional catalyst that composed of Fe-based catalytic component and acidic zeolite H-ZSM-5 is highly effective for valuable chemicals (aromatics, alkenes, and iso-paraffins) synthesis from CO_2 hydrogenation with alkenes as the key reaction intermediates via the cascade reaction including the reverse water gas shift (RWGS), Fischer-Tropsch synthesis (FTS), and acidic zeolite-catalyzed aromatization, cracking, or isomerization reaction, herein denoted as modified FTS pathway [16–19]. During the modified FTS pathway, the physicochemical property of H-ZSM-5 plays a vital role in determining the product distribution. Sun et al. employed a multifunctional catalyst Na-Fe_3O_4/H-ZSM-5 to realize the direct conversion of CO_2+H_2 into gasoline fuel or aromatics by regulating the Brønsted acid site property of H-ZSM-5 [16,17]. In the previous work from our research group, we designed a hollow H-ZSM-5 zeolite to combine with the Na-Fe@C catalyst for the modified FTS CO_2 conversion. The hollow H-ZSM-5 zeolite with short diffusion channels, appropriate density and strength of acid sites guaranteed the high yield of aromatics [18]. Sun et al. combined the Na-modified spinel oxide ZnFeOx and hierarchical nanocrystalline H-ZSM-5 aggregates for valuable chemicals synthesis from CO_2 hydrogenation. Benefiting from the appropriate density of Brønsted acid site, outstanding aromatics yield, and high catalytic stability were achieved [19].

Even though the modified FTS pathway has shown great potential for high-yield synthesis of value-added chemicals from CO_2 hydrogenation and tremendous progress has been made in the rational design of multifunctional catalysts, the structure-function relationship in the multi-component catalytic materials, especially the effect of physicochemical property of H-ZSM-5 on the product distribution, is still under ambiguous. The work reported so far mainly focused on the effect of Brønsted acid site density and strength on the product distribution, and the deep reason for the variation of product selectivity has been rarely clarified in detail [16,17,19,20]. As we know, the acidic property of H-ZSM-5 is actually dependent on the location and coordination environment of Al in the channel of zeolite crystal, which is sensitive to the synthesis raw agents (Si and Al resources) and conditions (hydrothermal time and temperature) [21–24]. Therefore, it is essential to pay more attention to the location and coordination environment of Al in H-ZSM-5 to clarify the structure-function relationship of modified FTS multifunctional catalyst in CO_2 hydrogenation.

In this work, we designed four kinds of H-ZSM-5 zeolites with different cases of Al location and corresponding acidic property by varying the synthesis raw agents and conditions. After combining with the Fe-based catalyst, obvious differences in product distribution were achieved from the different multifunctional catalysts. With the help of multiple advanced characterizations and theoretical calculations, the structure-function relationship between H-ZSM-5 and product distribution in modified FTS CO_2 hydrogenation was well built: the skeleton Al species at the intersection of straight and sinusoidal channels is beneficial for aromatics synthesis, whereas the straight or sinusoidal channels skeleton Al-induced Brønsted acid sites could boost the isomerization reaction, therefore resulting in iso-paraffins as the main product.

2. Experimental section

2.1. Catalyst preparation

2.1.1. Materials and chemicals

Iron nitrate nonahydrate [$Fe(NO_3)_3{\cdot}9\ H_2O$], aluminum nitrate nonahydrate [$Al(NO_3)_3{\cdot}9\ H_2O$], aluminum sulfate octadecahydrate [$Al(SO_4)_3{\cdot}18\ H_2O$], aluminum isopropoxide, sodium aluminate ($NaAlO_2$), sulfuric acid (H_2SO_4), anhydrous sodium carbonate (Na_2CO_3), sodium hydroxide (NaOH), ammonium nitrate (NH_4NO_3), triethylenediamine, tetraethyl orthosilicate (TEOS), ethanol, dimethyl formamide (DMF), and 1,4-benzene dicarboxylic acid were purchased from Wako Pure Chemical Corporation. Colloidal silica (LUDOX® AS-30, 30 wt% suspension in H_2O) and tetrapropylammonium hydroxide (TPAOH) were purchased from Sigma-Aldrich Corporation and TCI Corporation, respectively. All of the reagents were used directly without further purification. The deionized water used for catalyst preparation with a resistivity of 18.2 megohms was prepared using an ultrapure water system.

2.1.2. Synthesis of Na-Fe@C catalyst

Na-Fe@C was prepared with Fe-based metal-organic frameworks (Fe-MOFs) as precursors [18]. Typically, $Fe(NO_3)_3{\cdot}9\ H_2O$ (4.0 mmol, 1.62 g) and triethylenediamine (2.0 mmol, 0.22 g) were dissolved in DMF (50 mL) by vigorous stirring. To the aforementioned solution, a DMF solution (10 mL) containing 1,4-benzene dicarboxylic acid of 0.70 g was added dropwise. After stirring for 1 h, the mixture was transferred into a Teflon-lined autoclave (80 mL) and kept at 120 °C for 24 h. The crystalline product was collected by centrifugation and washed three times by DMF. The Fe-MOFs were obtained after drying the crystalline product at 60 °C overnight in a vacuum oven. Fe@C catalyst was fabricated by pyrolysis of Fe-MOFs at 550 °C for 3 h under a N_2 atmosphere with a heating rate of 2 °C min^{-1}. Na-Fe@C with 0.47 wt % Na (determined by X-ray fluorescence spectrum) was prepared by a wetness impregnation method with Na_2CO_3 as Na source.

2.1.3. Preparation of H-ZSM-5 zeolites

H-ZSM-5 zeolite with ellipsoidal morphology (Z-5-Ellipsoid) was synthesized according to the method reported by Rownaghi et al. with some modifications [25]. The molar ratio of Si and Al sources was kept at ca. 70. Typically, the aluminum isopropoxide was added into an aqueous mixture of TPAOH and NaOH under vigorous stirring at room temperature until a clear solution formed. Then, the above solution was added into the polypropylene bottle containing TEOS. After stirring for several hours, the clear solution was transferred into a Teflon-lined autoclave and hydrothermally treated at 160 °C for 24 h. The white crystals were recovered by centrifuging at 15000 rpm for 30 min and washing four times with water. After drying the white crystals, the organic template was removed by calcination at 550 °C for 5 h in air.

For the preparation of H-ZSM-5 zeolite aggregated by nanocubes (Z-5-Aggregate), the seeding gel was first synthesized as the following procedure [26]. The colloidal silica (30 wt% suspension in H_2O) was added dropwise into TPAOH (25% in water) for 2 h under stirring at room temperature. Then the mixture was put into a Teflon-lined autoclave and hydrothermally treated at 100 °C for 24 h. The obtained seeding gel was employed directly for the preparation of Z-5-Aggregate without any treatments. Typically, NaOH and $NaAlO_2$ were dissolved in a certain amount of deionized water, and then the seeding gel and colloidal silica were dropwise added into the clear solution subsequently. After stirring for 2 h, the mixture with a Si/Al molar ratio of ca. 70 was transferred into a Teflon-lined autoclave and kept at 180 °C for 24 h. Z-5-Aggregate was obtained after centrifuging, drying, and calcining at 550 °C for 5 h in air. It should be noted that the H-type Z-5-Aggregare was obtained after ion-exchanging in an aqueous solution of NH_4NO_3 (1 mol/L) for three times, and calcining at 550 °C for 5 h in air.

The diquaternary ammonium-type surfactant [$C_{18}H_{37}$-$N^+(CH_3)_2$-$(CH_2)_6$-$N^+(CH_3)_2$-C_6H_{13}]Br_2 (simplified as $C_{18-6-6}Br_2$) was employed to fabricate the H-ZSM-5 zeolite with pillared nanosheet (Z-5-Sheet) following the method reported by Ryoo et al. with some modification [27,28]. In a typical synthesis, NaOH (1.6 g, 0.04 mol) and structure-directing agent $C_{18-6-6}Br_2$ (4.42 g) were simultaneously dissolved in the deionized water (36 mL), and the mixture was stirred at room temperature for 20 min to form a homogeneous solution A. Then, H_2SO_4 (1.0 g, 98 wt%) and $Al_2(SO_4)_3{\cdot}18\ H_2O$ (0.9 g) were dissolved in the deionized water with the help of magnetic stirring to obtain solution

B. Next, the solution B was dropwise added into solution A under vigorous stirring maintained at 60 °C for 1 h. After cooling to room temperature, TEOS was added and stirred for 1 h, and the Si/Al ratio was controlled at ca. 70. After that, the homogeneous solution was transferred into a Teflon-lined autoclave and hydrothermally treated at 150 °C for 216 h. The Z-5-Sheet zeolite was obtained after centrifuging, washing with deionized water for three times, drying at 100 °C overnight, and calcining at 550 °C for 5 h in air.

H-ZSM-5 with hexagonal morphology (Z-5-Hexagon) and Si/Al ratio of 70 was prepared by the following method. Typically, a certain amount of $Al(NO_3)_3{\cdot}9\ H_2O$ (0.6 g), TPAOH (15.6 g), TEOS (16.6 g), and ethanol (15.6 g) were dissolved in the deionized water. After magnetic stirring for 4 h, the resultant clear solution was transferred into a Teflon-sealed autoclave and maintained at 180 °C for 24 h under static condition. After cooling down to room temperature, the white product was washed with deionized water for three times and dried at 60 °C overnight. The organic template was removed by calcination at 550 °C for 5 h in air.

The multifunctional catalyst Na-Fe@C/Z-5-X (X = Ellipsoid, Aggregate, Sheet, or Hexagon) was fabricated by uniformly mixing pelletized Na-Fe@C (0.1 g, 20–40 mesh) and Z-5-X (0.3 g, 20–40 mesh) in a vessel, then placed them in a single bed.

2.2. Catalyst characterizations

A Rigaku RINT 2400 X-ray diffractometer (XRD) with Cu Kα radiation was used to record the crystal structure of the catalysts. The specific surface area and pore size distribution of the catalysts were measured on a Micromeritics 3Flex 2MP instrument. Prior to the experiment, the samples were degassed at 200 °C for 10 h. The specific surface area was calculated by the Brunauer-Emmett-Teller (BET) method, the average pore size and pore volume were calculated according to the Barrett-Joyner-Halenda (BJH) method. Horváth-Kawazoe (HK) and BJH methods were employed to analyze the pore size distribution of microporous and mesoporous, respectively. The temperature-programmed desorption of NH_3 (NH_3-TPD) was performed on a Microtrac BELCATII-T-SP equipment to evaluate the amount of acid sites in Z-5-X. Typically, the catalyst (0.05 g) was pretreated in a flow of pure He at 150 °C for 1 h. Then the sample was NH_3-saturated at 50 °C. After cleaning up the physically adsorbed NH_3 by a He flow, the NH_3-TPD curves were recorded under the He flow with a heating rate of 10 °C min^{-1}. Pyridine-adsorbed Fourier transform infrared (Py-FTIR) spectra was performed on a Bruker Tensor 27 FTIR spectrometer to distinguish the acid type in Z-5-X. Prior to the Py-FTIR test, the zeolite was pressed into a self-supported wafer and degassed at 400 °C and 10^{-4} Pa for 1 h. After that, inert gas was saturated with pyridine and was introduced into the IR cell for 1 h at room temperature. Finally, the Py-FTIR spectra were collected when the catalyst was heated to 150 °C with a heating rate of 10 °C min^{-1}. The elemental contents in the catalysts were measured by a Phillips 2400 X-ray fluorescence (XRF) spectrometer. The morphology of the catalysts was observed by a transmission electron microscopy (TEM, JEM-2100UHR, JEOL) and a scanning electron microscopy (SEM, JSM-6700 F, JEOL). ^{27}Al solid-state magic angle spinning nuclear magnetic resonance (MAS NMR) was carried out on the Bruker Avance 400WB spectrometer.

2.3. Catalytic activity evaluation

The catalytic performance was tested in a continuously fixed bed reactor equipped with a cold trap (0 °C). The catalyst was loaded in the middle of the reactor with quartz wool and reduced with H_2 at 400 °C for 8 h prior to the reaction. After cooling down to room temperature, the gas-phase reactants (24.3% CO_2, 71.8% H_2, and 3.9% Ar) were fed into the reactor, and the reaction temperature and pressure were maintained at 320 °C and 3 MPa, respectively. The products in the gas phase were examined using two online gas chromatographs (GC, Shimadzu GC-2014), one of which equipped with a thermal conductive detector (TCD) and an active charcoal column for the measurement of CO_2, CO, Ar, and CH_4, and another one equipped with a flame ionization detector (FID) and a Porapak-Q column for the analysis of gas-phase hydrocarbons. The heavy hydrocarbons collected by the cold trap were analyzed by an off-line GC (Shimadzu GC-2014) equipped with a DB-1 capillary column and an FID. The carbon balances in all catalytic runs were within 92–105%. Experimental data were discussed after reaction of 24 h. The CO_2 conversion and hydrocarbon distribution were calculated according to the following equations:

$$CO_2 Conversion = \frac{CO_{2inlet} - CO_{2outlet}}{CO_{2inlet}} \times 100\%$$

Where CO_{2inlet} and $CO_{2outlet}$ represent moles of CO_2 at the inlet and outlet, respectively.

$$Sel_{C_nH_m} = \frac{nC_nH_m\ _{outlet}}{\sum_1^n nC_nH_m\ _{outlet}} \times 100\%$$

Where n represents the carbon number of product C_nH_m.

$$CO\quad selectivity = \frac{CO_{outlet}}{CO_{2inlet} - CO_{2outlet}} \times 100\%$$

Where CO_{outlet} represents the mole of CO at the outlet.

2.4. Computational Simulations

The VASP package was used to carry out all the calculation [29,30]. The interaction between electrons and ions was characterized using the projector augmented wave (PAW) technique [31]. The calculations were performed using the Perdew-Burke-Ernzerhof (PBE) function [32]. The cutoff for the kinetic energy of the pane wave is 400 eV. The sampling of Brillouin zone was only with gamma point. Throughout every structure optimization, the threshold of force and energy convergence were 0.03 eV/Å and 1.0×10^{-4} eV. DFT-D3 was utilized to account for the long-range van der waals dispersion interaction between the adsorbate and H-ZSM-5 [33].

A periodic orthorhombic cell made up of 96 T atoms was used to model the H-ZSM-5 [34]. Two models were established to represent the various reaction positions, including the framework aluminum atom was situated at the straight channel and intersection channel separately during the alkene aromatics reaction. Furthermore, for alkene iso-paraffins reaction, three models were constructed corresponding to one, two, and three B acid sites located at the straight channel by substituting skeleton Si with Al, respectively. The optimized lattice constants are a=19.09 Å, b=19.62 Å and c=12.86 Å. All atoms within the cell were let to relax while the lattice constants were held constant. The climbing image nudged elastic band (CI-NEB) method was combined with the dimer method to search for all transition states [35]. The transition state structure was optimized until the forces on the atom were reduced to 0.05 eV/Å.

The reaction energy(ΔE) and barrier (Eact) are calculated via Eqs. (1) and (2):

$$\Delta E = E_{FS} - E_{IS} \tag{1}$$

$$E_{act} = E_{TS} - E_{IS} \tag{2}$$

Where E_{IS}, E_{TS}, and E_{FS} are the total energy of the corresponding initial state (IS), transitional state (TS), and final state (FS), respectively.

3. Results and discussion

3.1. Physicochemical property of Fe-based catalyst before and after CO_2 hydrogenation reaction

The Fe-based active sites, including iron oxide (mainly Fe_3O_4) for

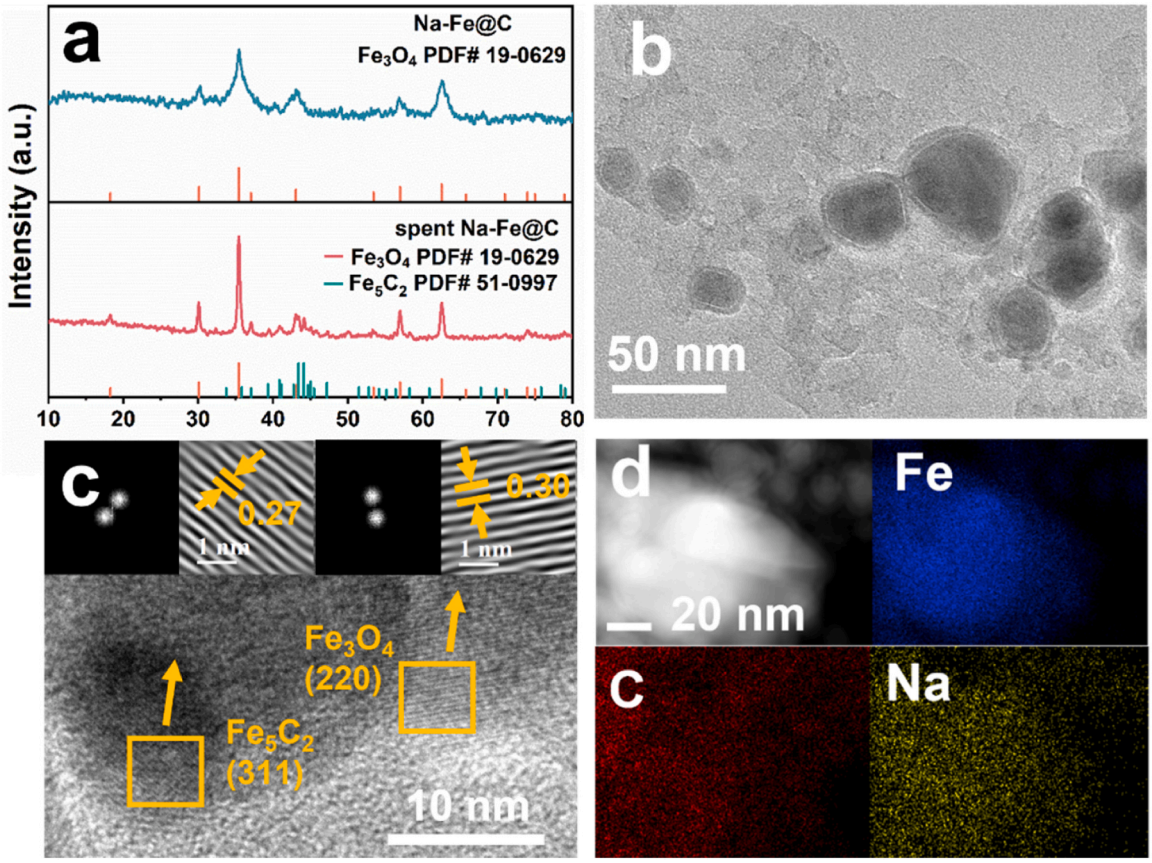

Fig. 1. (a) The XRD patterns of the fresh Na-Fe@C and the spent Na-Fe@C catalysts. (b-c) The TEM and HRTEM images of the spent Na-Fe@C. (d) HAADF-STEM image of the spent Na-Fe@C catalyst and elemental mapping of C, Fe, and Na elements.

reverse water-gas shift reaction (RWGS, $CO_2 + H_2 \rightarrow CO + H_2O$) and iron carbide (mainly Fe_5C_2) for alkenes synthesis via C-C coupling, are key components in the multifunctional catalyst, and their physicochemical properties are the prerequisites for the catalytic performance of CO_2 hydrogenation. Here, a carbon supported Fe-based catalytic component denoted as Na-Fe@C was prepared by carbonizing the Fe-based metal-organic frameworks (MOFs) under a N_2 atmosphere and doping of alkali metal Na. The XRD patterns (Fig. 1a) confirmed that Fe-based active sites in the fresh Na-Fe@C existed in the form of magnetite Fe_3O_4 (PDF#19–0629). The sole Na-Fe@C catalyst delivered high alkenes selectivity of 70.6% at a CO_2 conversion of 30.6% under 320 °C and 3 MPa, therefore supplying essential intermediates for targeted product synthesis on the second catalytic component acidic zeolite. During the CO_2 hydrogenation process, the crystal phase of Na-Fe@C underwent tremendous changes with χ-Fe_2C_5 (PDF#51–0997) appeared due to the carburization effect endowed by the in-situ formed CO from RWGS reaction. Benefiting from the carbon supported structure of Na-Fe@C, the Fe-based nanoparticles were dispersed well after reaction as shown in the transmission electron microscopy (TEM, Fig. 1b) image. The crystal plane of Fe_3O_4 (220) with interspace of 0.30 nm and Fe_5C_2 (311) with interspace of 0.27 nm could be resolved from the high-resolution TEM (HRTEM, Fig. 1c) images, which confirms the co-existence of Fe_3O_4 and Fe_5C_2 in the spent catalyst and corresponds well with the XRD results. As shown in the high-angle annular dark-field scanning TEM (HAADF-STEM) elemental mapping images (Fig. 1d), the Fe-based active sites were mainly anchored on the nanoparticles, whereas the Na and C elements were evenly distributed on the whole substrate. Specially, the homogeneous distribution of Na is beneficial for the desorption of alkenes due to the similar electron-donating effect with alkenes, therefore boosting alkenes synthesis [36].

3.2. Physicochemical property of Z-5-X zeolite obtained from different methods

Four types of Z-5-X zeolites (Z-5-Ellipsoid, Z-5-Aggregate, Z-5-Sheet, and Z-5-Hexagon) were prepared by varying the raw synthesis materials and hydrothermal conditions. The Si/Al ratio of the four Z-5-X zeolites was controlled in the narrow range of 65–72 as confirmed by X-ray fluorescence spectroscopy (XRF, Table S1), and the X-ray diffraction (XRD, Fig. S1) pattern of Z-5-X corresponded well to the MFI structure (PDF#44–0003). The morphology and the texture property are shown in the Fig. S2-S6 and Table S1, and the detailed discussion is given in the supporting information. As the main origin of acidic site in Z-5 zeolite, the location of Al species, such as at the straight/sinusoidal channels or at the intersection of them, plays an essential role in varying the catalytic performance owing to the different confined cavities, as shown in Fig.2a [37–39]. Here, the synthesis conditions (hydrothermal time and temperature) and raw materials (organic template and Si/Al resources) delivered disparate Al location in the channels of Z-5-X, thus altering the selectivity of targeted product from CO_2 conversion effectively. The location environment of Al species was investigated by ^{27}Al solid-state magic angle spinning nuclear magnetic resonance (MAS NMR, Fig. 2b-f). Two peaks located at 0 and 55 ppm were observed in all of the Z-5-X zeolites, and the former one could be assigned to the extra-framework Al species, whereas the latter one might originate from the framework Al with tetrahedral coordination type [40]. The strong peak intensity at 55 ppm but weak peak intensity at 0 ppm confirmed that the tetrahedrally coordinated Al species were dominant in all of Z-5-X. Moreover, the ^{27}Al NMR peak at 55 ppm can be deconvoluted into five satellite peaks that are centered at 52, 53, 54, 56, and 58 ppm, respectively [41,42]. Typically, the peak at 54 ppm corresponded to the framework Al located at the intersection of straight and sinusoidal

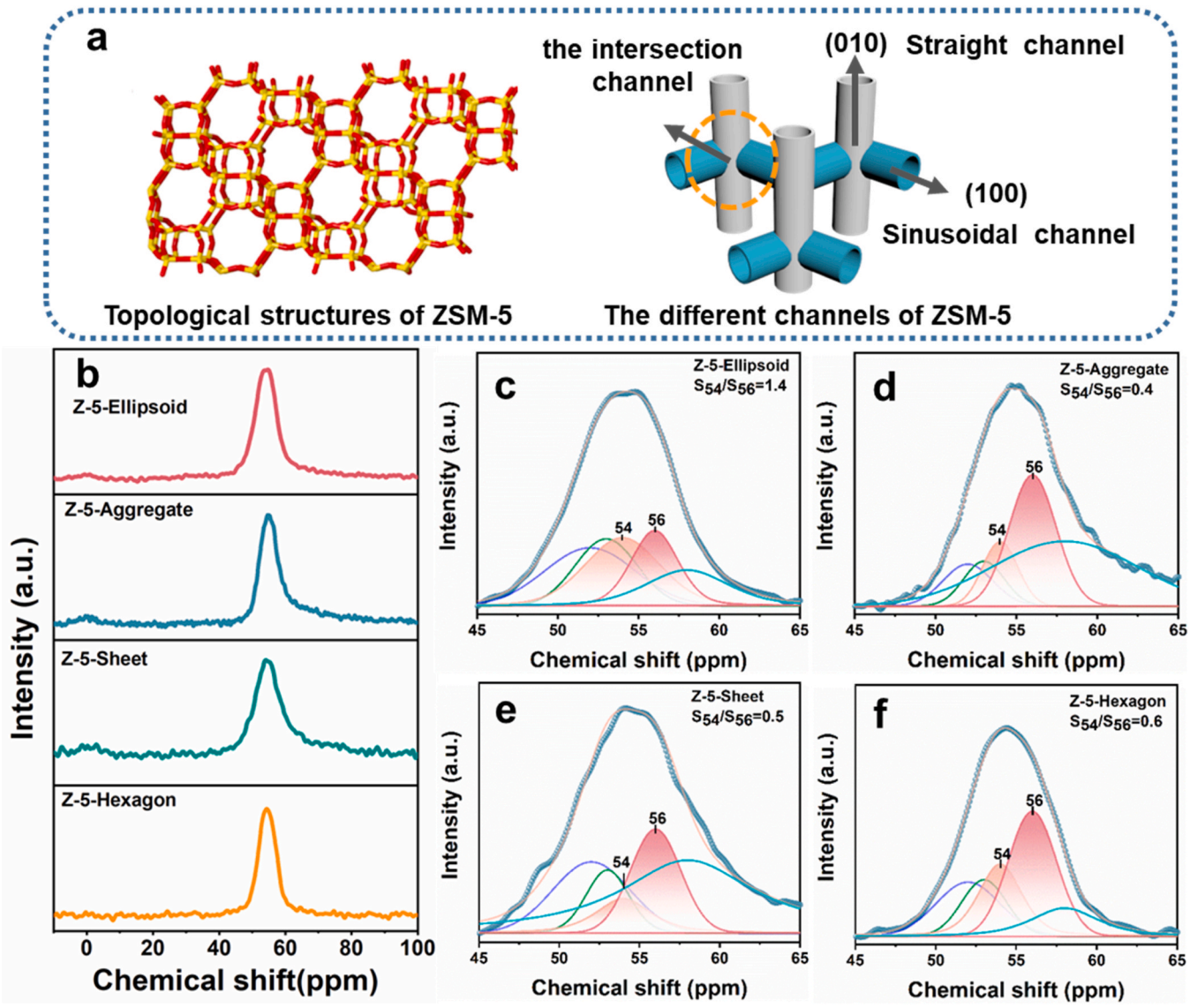

Fig. 2. (a) Topological structure and corresponding channels of ZSM-5. (b-f) ^{27}Al MAS NMR spectra of Z-5-X.

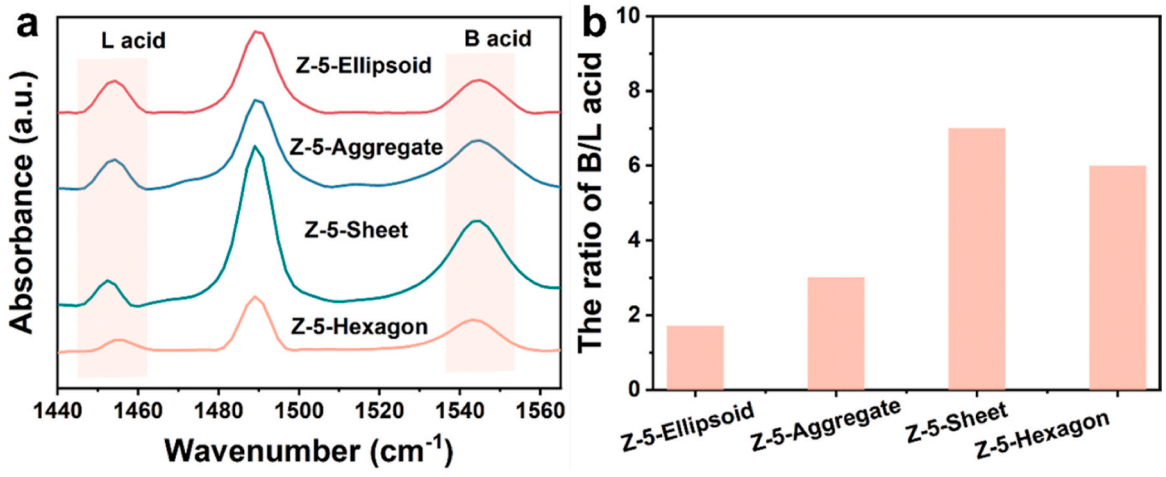

Fig. 3. (a) Py-IR spectra of Z-5-X zeolites. (b) The ratio of B/L in Z-5-X zeolites.

Table 1
The acidic property of Z-5-X zeolites prepared by different methods.

Sample	Acid site amount (μmol/g)			Acid site type and amount (μmol/g) measured by Py-IR			Al_{54}/ A_{56}
	W	M+S	Total	Brønsted acid	Lewis acid	B/L	
Z-5-Ellipsoid	17.0	34.0	51.0	19.5	11.8	1.7	1.4
Z-5-Aggregate	19.0	41.0	60.0	23.8	8.2	3.0	0.4
Z-5-Sheet	17.0	52.0	69.0	44.1	6.3	7.0	0.5
Z-5-Hexagon	18.0	24.0	42.0	19.5	3.3	6.0	0.6

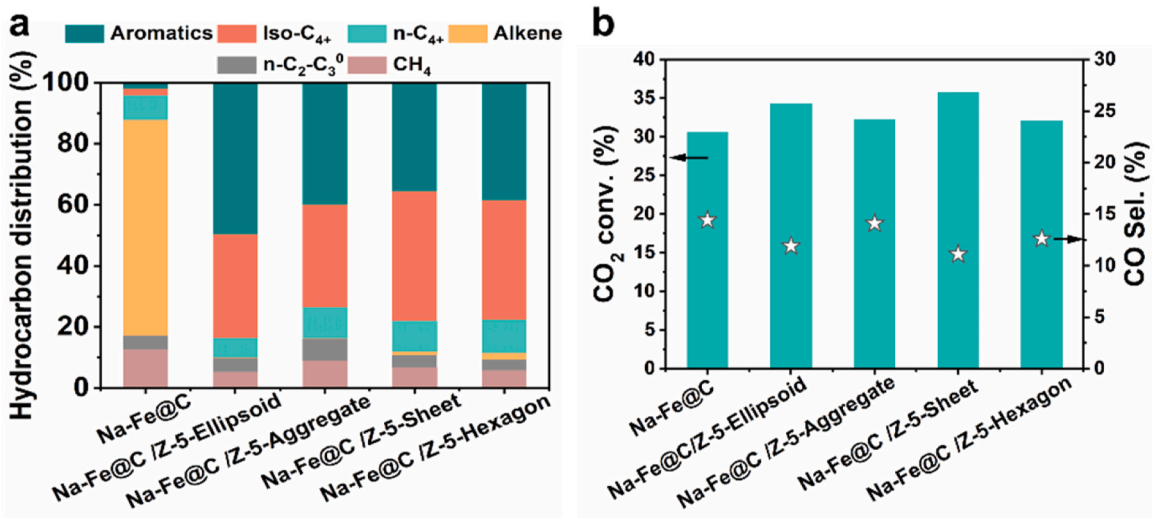

Fig. 4. (a) The hydrocarbon distribution of Na-Fe@C/Z-5-X. (b) CO_2 conversion and CO selectivity of Na-Fe@C/Z-5-X.

channels, while the peak at 56 ppm was derived from the framework Al located at either the straight or sinusoidal channel [41,42]. Among all of the Z-5-X zeolites, Z-5-Ellipsoid exhibited the highest peak area ratio of Al_{54}/Al_{56} (1.4), indicating that much more Al species were distributed at the intersection of straight and sinusoidal channels. For the other three samples, the peak area ratios of Al_{54}/Al_{56} were all lower than 1 due to the preferential location of Al at either the straight or sinusoidal channel.

The acidic property of Z-5-X endowed by the Al coordination environment is a direct descriptor of the catalytic performance. First, the acidic property was examined by NH_3-temperature programmed desorption (NH_3-TPD, Fig. S7). All the Z-5-X displayed two NH_3 desorption peaks at the temperature ranges of 100–250 and 250–400 °C, which correspond to the weak and medium + strong acid sites, respectively. The variation of NH_3 desorption peak area confirmed that the acid site quantity of Z-5 Ellipsoid, Z-5-Aggregate, Z-5-Sheet, and Z-5-Hexagon was 51.0, 60.0, 69.0, and 42.0 μmol g^{-1}, respectively. More detailed, the acid type and the corresponding amount in Z-5-X were distinguished by pyridine-adsorbed Fourier transform infrared (Py-FTIR) spectra. As shown in the Py-FTIR curves of Z-5 zeolites (Fig. 3a), three typical peaks at 1455, 1490, and 1545 cm^{-1} were detected, which can be assigned to the Lewis acid sites, both of Lewis and Brønsted acid sites, and Brønsted acid sites, respectively [43]. Different from the Brønsted acid that is associated with the tetrahedral framework Al in the form of a bridging hydroxyl (Si-OH-Al) in Z-5 zeolite, the Lewis acid is generally derived from the extra-framework Al [44]. The appearance of typical IR peak that corresponding to Brønsted acid was originated from the combination of proton in Brønsted acid with pyridine for pyridinium ion formation, and the IR peak of Lewis acid was due to the dehydroxylation of zeolite [45]. Quantitatively, Z-5-Aggregate, Z-5-Sheet, and Z-5-Hexagon exhibited high Brønsted acid concentration relative to the Lewis acid with the quantity ratio of Brønsted acid to Lewis acid (B/L) higher than 3.0 (Fig. 3b, Table 1). Specially, Z-5-Sheet delivered the highest Brønsted acid concentration (44.1 μmol g^{-1}) and B/L ratio of 7.0, which will bring special product distribution from CO_2 hydrogenation. It should be noted that the difference in the amount of acid site determined by NH_3-TPD and Py-FTIR was due to the different accessibilities of probe molecules (pyridine and NH_3) with different molecule sizes to the acid sites [43].

3.3. The structure-function relationship of Z-5-X in CO_2 hydrogenation

Z-5-X was combined with the Na-Fe@C catalytic component to realize the direct conversion of CO_2 + H_2 into valuable chemicals in a one-pass under given reaction conditions (320 °C, 3 MPa, 9000 mL·gNa-Fe@C^{-1}·h^{-1}, and 24 h). Owing to the complicated acidic zeolite-catalyzed reactions, including oligomerization, dehydrogenation, aromatization or isomerization, the main product of alkenes from Na-Fe@C altered into various chemicals, such as paraffins, iso-paraffins, aromatics, etc., after introducing acidic zeolite into the catalytic system (Fig. S8, Table S2, Fig. 4a). Compared with the sole Na-Fe@C catalytic component, the CO_2 conversion achieved from the multifunctional catalyst Na-Fe@C/Z-5-X was enhanced in different degrees due to the continuous consumption of reaction intermediates on the acidic zeolite and the forward shift of the reaction equilibrium. Typically, higher CO_2 conversion was achieved from Na-Fe@C/Z-5-Ellipsoid (34.3%) and Na-Fe@C/Z-5-Sheet (35.8%). It is obvious that aromatics and iso-paraffins were the main products from all the multifunctional catalysts Na-Fe@C/Z-5-X, which will be employed as two indicators to illustrate the structure-function relationship of Z-5-X in the following statement.

For targeted product synthesis, Na-Fe@C/Z-5-Ellipsoid exhibited the highest aromatics selectivity of 49.6% compared with the other multifunctional catalysts. Comprehensively considering the Al location environment and acidic property of Z-5 zeolites, Z-5-Ellipsoid displayed tremendously different Al species distributions with the highest ratio of Al_{54}/Al_{56} (1.4), therefore much more Al species that located at the intersection of straight and sinusoidal channels of Z-5-Ellipsoid might be

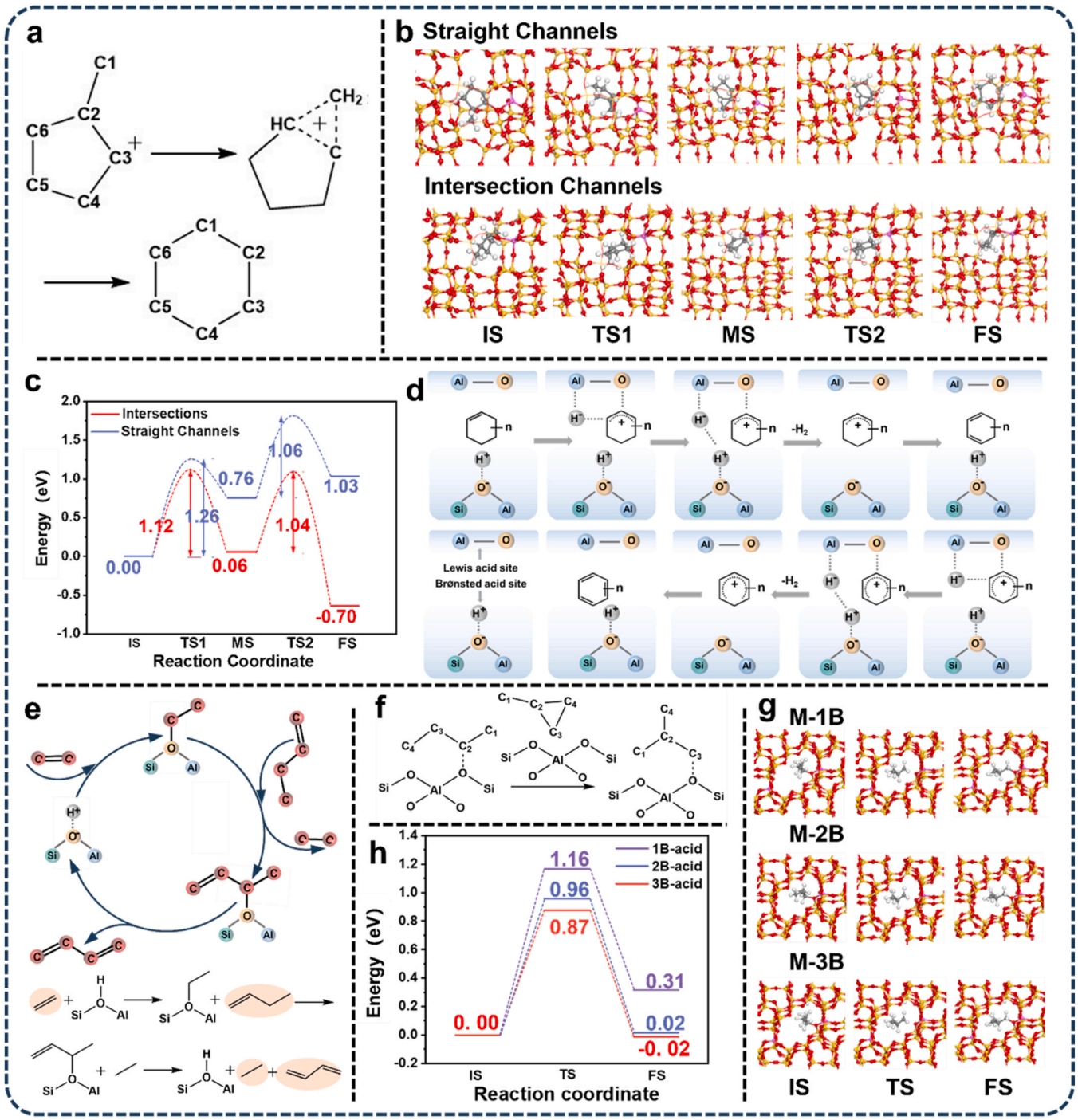

Fig. 5. (a) The representative elementary step of the ring expansion of cyclopentyl into cyclohexyl. (b) Computational models that represent the different acid site positions in Z-5 zeolite. (c) Reaction energy profiles of cyclopentyl to cyclohexyl in intersection channel and straight channel. (d) The synergistic effect between the Lewis and Brønsted acid sites for the dehydrogenation route in the aromatization process. (e) Typical hydrogen transfer pathway on Brønsted acid sites. (f) The representative skeletal isomerization step 2-butoxide transforms into isobutoxide. (g) Computational models that represent the different B-acid sites amount in Z-5 zeolite. (h) Reaction energy profiles of alkene skeletal isomerization.

beneficial for aromatics synthesis. Compared with the active sites at the straight and sinusoidal channels that inclined to crack or isomerize the intermediates due to the confinement effect, the acidic sites at the channel intersection of Z-5 zeolites with a larger reaction cavity could provide sufficient space for aromatization. We evaluated the capability of aromatization reaction at different positions of Z-5 zeolites with the aid of density functional theory (DFT) calculation, in which the representative elementary step of the ring expansion of cyclopentyl into cyclohexyl was employed to simulate the aromatization process (Fig. 5a) [46,47]. Two models were built (Fig. 5b and Fig. S9-S10) to represent the different reaction positions, including the models with one Brønsted acid site at the straight channel and at the channel intersection. The ring expansion of cyclopentyl into cyclohexyl process contained two essential transition states. As shown in Fig. 5c and Tables S3-S4, for the straight channel model, the energy barriers of 1.26 and 1.06 eV were required to complete the ring expansion process. Interestingly, the energy barriers decreased to 1.12 and 1.04 eV for the intersection channel model, which indicates that the elementary step is more probable to

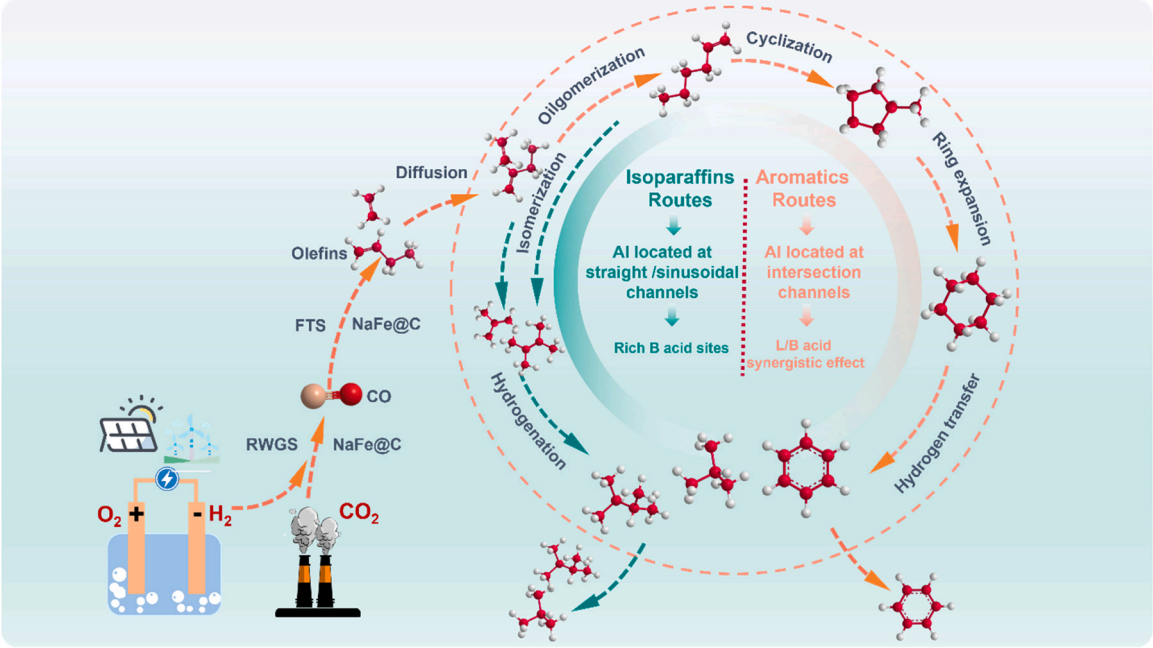

Fig. 6. Scheme of product distribution tailoring via Z-5 zeolites with different Al location and acidic property.

occur in this model. Based on the experimental and simulation results, it is reasonable to believe that the Al located at the intersection position hold great potential to boost the aromatics synthesis.

It has been widely accepted that the cooperative interaction between the Brønsted and Lewis acid sites plays a unique role in controlling the aromatics selectivity [48,49]. There are two H-subtraction pathways during the aromatic synthesis process, including the dehydrogenation route with H_2 molecule release and the H-transfer route from H-donors to H-acceptors [50,51]. For the Brønsted and Lewis acid sites co-dominated dehydrogenation route, the release of H_2 could efficiently boost the aromatics selectivity by avoiding the undesirable consumption of aromatics synthesis intermediates. As shown in Fig. 5d, the Lewis acid site first subtracts H- species from the intermediates. Then the combination of H- with the proton in Brønsted acid site guarantees H_2 molecule formation. Finally, the deprotonation of the carbenium ion ensures the recovery of the Brønsted acid site. However, the H-transfer route dominantly mediated by the Brønsted acid sites could employ the aromatics synthesis intermediates, e.g., alkenes or cycloalkenes, as H-acceptors, thus leading to low aromatics selectivity (Fig. 5e).

The synergistic effect between Brønsted and Lewis acid sites as discussed above can be deeply re-understood by the varied aromatics selectivity obtained from Na-Fe@C/Z-5-X multifunctional catalysts. On the one hand, the inferior aromatics selectivity obtained from Na-Fe@C/Z-5-Aggregate, Na-Fe@C/Z-5-Hexagon, and Na-Fe@C/Z-5-Sheet could be attributed to the low Brønsted acid concentration in the channel intersection of Z-5 zeolites as indicated by the low ratio of Al_{54}/Al_{56} (0.4–0.6). On the other hand, the appropriate concentration ratio between the Brønsted and Lewis acid sites is also responsible for improving the aromatics selectivity. The aromatics selectivity change sequence of Na-Fe@C/Z-5-Aggregate (39.9%) > Na-Fe@C/Z-5-Hexagon (38.6%) > Na-Fe@C/Z-5-Sheet (35.6%) was consistent with the variation trend of B/L ratio in these three Z-5 zeolites, Z-5-Aggregate (B/L=3.0), Z-5-Hexagon (B/L=6.0), Z-5-Sheet (B/L=7.0). The imbalance between the quantity of Brønsted and Lewis acid sites, especially too many Brønsted acid sites, could make the H-transfer route from H-donors to H-acceptors more dominant than the dehydrogenation route during the aromatic synthesis process, therefore facilitating the consumption of aromatics synthesis intermediates and lowering the aromatics selectivity. Thus, we can conclude that both adequate Brønsted acid sites at the channel intersections and the appropriate amount balance between the Brønsted and Lewis acid sites are essential for aromatics synthesis.

Interestingly, owing to the unique acidic property of Z-5-Sheet, the multifunctional catalyst Na-Fe@C/Z-5-Sheet exhibited excellent iso-paraffins selectivity of 42.5% at a CO_2 conversion of 35.8%. It is worth noting that the skeletal isomerization of alkene is the rate-limiting step for iso-paraffins synthesis, which heavily depends on the density and location of Brønsted acid sites [52–55]. First, Z-5-Sheet with a large number of Brønsted acid sites located at the straight or sinusoidal channel (Al_{54}/Al_{56} = 0.5) is favorable for iso-paraffins synthesis. Compared with the channel intersection, the Brønsted acid sites at the straight or sinusoidal channel with stronger confinement effect make the intermediates more likely to be cracked or isomerized into iso-paraffins. Second, the Brønsted acid concentration is another key factor in enhancing the selectivity of iso-paraffins. We further assessed the effect of Brønsted acid density on the isomerization of alkenes with the aid of DFT calculation. The representative skeletal isomerization step that 2-butoxide intermediate transforms into isobutoxide intermediate was employed to stimulate the isomerization process (Fig. 5f) [54]. Three models were constructed to represent the different Brønsted acid densities in the straight channel, including one, two, and three Brønsted acid sites, defined as M-1B, M-2B, M-3B. (Fig. 5g and Fig. S11-S13). As shown in Fig. 5h and Table S5, the reaction energy barriers of 1.16, 0.96, and 0.87 eV were needed for the three models, respectively, to complete the isomerization process. It is obvious that the high Brønsted acid density in the straight or sinusoidal channel has considerable potential to improve iso-paraffins synthesis. It should be noted that iso-paraffins are ideal additives to enhance the octane number of gasoline fuels [56,57].

Based on the multiple characterization and theoretical calculations, we proposed a feasible reaction scheme for tandem catalysis of CO_2+H_2 into valuable chemicals via multifunctional catalysts Na-Fe@C/Z-5-X (Fig. 6). First, the RWGS reaction on Fe_3O_4 and FTS process on χ-Fe_5C_2 guarantee the formation of alkenes, which can be employed as key intermediates for targeted product synthesis with the aid of acidic zeolite Z-5. Due to the co-existence of Fe_3O_4 and χ-Fe_5C_2 in Fe-based catalyst, the direct transformation of CO_2+H_2 into alkenes can be realized via a sole catalytic component. Subsequently, the generated alkenes diffuse into the channels of Z-5, in which complicated reactions, such as oligomerization, isomerization, aromatization, etc., occur. As a result of

the larger reaction cavity, the Brønsted acid sites at the intersection of straight and sinusoidal channels facilitate the aromatics formation by reducing the resistance of aromatization. The cooperative interplay between Brønsted and Lewis acid sites also plays an essential role in boosting aromatics selectivity. Conversely, compared to the channel intersections, the Brønsted acid sites at the straight or sinusoidal channel possess more constrained effects on aromatization, thus lowering the aromatics selectivity. Notably, when the aromatics diffuse out of the zeolite channels, side reactions, such as hydrocracking and isomerization, may occur at the external acid sites to alter the main product from aromatics to iso-paraffins, which can be well verified by the high iso-paraffins selectivity of 39.0% from Na-Fe@C/Z-5-Hexagon. More importantly, the excessive Brønsted acid sites at the straight or sinusoidal channel are inclined to enhance the iso-paraffins selectivity as confirmed by the high iso-paraffins selectivity of 42.5% from Na-Fe@C/Z-5-Sheet. Based on the discussion above, changing the Al location and acidic property of Z-5 could precisely control the product distribution of CO_2 hydrogenation.

4. Conclusions

In summary, we systematically investigated the influence of Al siting in zeolite channels and the corresponding acidity on the product distribution of CO_2 hydrogenation. Since the Brønsted acid sites at the channel intersection possess a larger space and less resistance to the transition state of aromatization step, it displays a higher capability for aromatics synthesis than that at the straight or sinusoidal channel. In addition, the well balance between the quantities of Brønsted and Lewis acid sites is another key factor boosting aromatics selectivity, otherwise excessive Brønsted acid sites would turn the main product into iso-paraffins by enhancing the alkene skeleton isomerization process. To the best of our knowledge, it is the first work that comprehensively reveals the effect of Al location and the corresponding acidic property of ZSM-5 zeolite on the product distribution from CO_2 hydrogenation.

CRediT authorship contribution statement

Xinhua Gao: Methodology. **Guohui Yang:** Methodology. **Ruosong He:** Data curation. **Shuhei Yasuda:** Formal analysis. **Jie Liang:** Investigation, Conceptualization. **Yang Wang:** Writing – review & editing, Writing – original draft, Supervision, Funding acquisition. **Mingbo Wu:** Supervision. **Noritatsu Tsubaki:** Funding acquisition, Formal analysis, Conceptualization. **Yongqiang Gu:** Writing – original draft, Formal analysis. **Kaixuan Huo:** Software. **Meng Li:** Software. **Wenhang Wang:** Investigation.

Declaration of Competing Interest

The authors declare that they have no known competing financial interests or personal relationships that could have appeared to influence the work reported in this paper.

Data availability

Data will be made available on request.

Acknowledgements

This work was financially supported by the National Key Research and Development Program of China (2023YFB4104500), the National Natural Science Foundation of China (22108310), the Science and Technology Innovation Project of the Shandong Energy Group Co., Ltd (SNKJ2023A03), the Foundation of State Key Laboratory of High-efficiency Utilization of Coal and Green Chemical Engineering (2022-KF-75), and the Japan Society for the Promotion of Science (JSPS) funds (22H01864, 23H05404). Y. Gu acknowledges the finical support from China Scholarship Council (CSC, 202208050051).

Appendix A. Supporting information

Supplementary data associated with this article can be found in the online version at doi:10.1016/j.apcatb.2024.123842.

References

[1] J. Rogelj, M. Elzen, N. Höhne, T. Fransen, H. Fekete, H. Winkler, R. Schaeffer, F. Sha, K. Riahi, M. Meinshausen, Paris Agreement climate proposals need a boost to keep warming well below 2 °C, Nature 534 (2016) 631–639, https://doi.org/10.1038/nature18307.
[2] D. Feldman1, W. Collins, P. Gero, M. Torn, E. Mlawer, T. Shippert, Observational determination of surface radiative forcing by CO_2 from 2000 to 2010, Nature 519 (2015) 339–343, https://doi.org/10.1038/nature14240.
[3] S. Xu, E. Carter, Theoretical insights into heterogeneous (photo)electrochemical CO_2 reduction, Chem. Rev. 119 (2019) 6631–6669, https://doi.org/10.1021/acs.chemrev.8b00481.
[4] S. Zhang, Q. Fan, R. Xia, T. Meyer, CO_2 reduction: from homogeneous to heterogeneous electrocatalysis, Acc. Chem. Res. 53 (2020) 255–264, https://doi.org/10.1021/acs.accounts.9b00496.
[5] J. Albero, Y. Peng, H. García, Photocatalytic CO_2 reduction to C2+ products, ACS Catal. 10 (2020) 5734–5749, https://doi.org/10.1021/acscatal.0c00478.
[6] Y. Wang, J. Sun, N. Tsubaki, Clever nanomaterials fabrication techniques encounter sustainable C1 catalysis, Acc. Chem. Res. 56 (2023) 2341–2353, https://doi.org/10.1021/acs.accounts.3c00311.
[7] J. Zhu, F. Cannizzaro, L. Liu, H. Zhang, N. Kosinov, I. Filot, J. Rabeah, A. Brückner, E. Hensen, Ni-In synergy in CO_2 hydrogenation to methanol, ACS Catal. 11 (2021) 11371–11384, https://doi.org/10.1021/acscatal.1c03170.
[8] Z. Li, W. Wu, M. Wang, Y. Wang, X. Ma, L. Luo, Y. Chen, K. Fan, Y. Pan, H. Li, J. Zeng, Ambient-pressure hydrogenation of CO_2 into long-chain olefins, Nat. Commun. 13 (1) (2022) 10, https://doi.org/10.1038/s41467-022-29971-5.
[9] Y. Wang, W. Wang, R. He, M. Li, J. Zhang, F. Cao, J. Liu, X. Gao, G. Yang, M. Wang, T. Xing, T. Liu, Q. Liu, H. Hu, N. Tsubaki, M. Wu, Carbon-based electron buffer layer on ZnOx-Fe_5C_2-Fe_3O_4 boosts enthanol synthesis from CO_2 hydrogenation, Angew. Chem. Int. Ed. 62 (2023) e202111786, https://doi.org/10.1002/ange.202311786.
[10] J. Ding, L. Huang, W. Gong, M. Fan, Q. Zhong, A. Russell, H. Gu, H. Zhang, Y. Zhang, R. Ye, CO_2 hydrogenation to light olefins with high-performance $Fe_{0.30}Co_{0.15}Zr_{0.45}K_{0.10}O_{1.63}$, J. Catal. 377 (2019) 224–232, https://doi.org/10.1016/j.jcat.2019.07.036.
[11] A. Noreen, M. Li, Y. Fu, C. Amoo, J. Wang, E. Maturura, C. Du, R. Yang, C. Xing, J. Sun, One-pass hydrogenation of CO_2 to multibranched isoparaffins over bifunctional zeolite-based catalysts, ACS Catal. 10 (2020) 14186–14194, https://doi.org/10.1021/acscatal.0c03292.
[12] P. Gao, S. Li, X. Bu, S. Dang, Z. Liu, H. Wang, L. Zhong, M. Qiu, C. Yang, J. Cai, W. Wei, Y. Sun, Direct conversion of CO_2 into liquid fuels with high selectivity over a bifunctional catalyst, Nat. Chem. 9 (2017) 1019–1024, https://doi.org/10.1038/nchem.2794.
[13] Y. Wang, L. Tan, M. Tan, P. Zhang, Y. Fang, Y. Yoneyama, G. Yang, N. Tsubaki, Rationally designing bifunctional catalysts as an efficient strategy to boost CO_2 hydrogenation producing value-added aromatics, ACS Catal. 9 (2019) 895–901, https://doi.org/10.1021/acscatal.8b01344.
[14] Z. Li, Y. Qu, J. Wang, H. Liu, M. Li, S. Miao, C. Li, Highly selective conversion of carbon dioxide to aromatics over tandem catalysts, Joule 3 (2018) 1–14, https://doi.org/10.1016/j.joule.2018.10.027.
[15] Y. Ni, Z. Chen, Y. Fu, Y. Liu, W. Zhu, Z. Liu, Selective conversion of CO_2 and H_2 into aromatics, Nat. Commun. 9 (2018) 1–7, https://doi.org/10.1038/s41467-018-05880-4.
[16] J. Wei, Q. Ge, R. Yao, Z. Wen, C. Fang, L. Guo, H. Xu, J. Sun, Directly converting CO_2 into a gasoline fuel, Nat. Commun. 8 (2017) 1–7, https://doi.org/10.1038/ncomms15174.
[17] J. Wei, R. Yao, Q. Ge, D. Xu, C. Fang, J. Zhang, H. Xu, J. Sun, Precisely regulating Brønsted acid sites to promote the synthesis of light aromatics via CO_2 hydrogenation, Appl. Catal. B 283 (2021) 119648, https://doi.org/10.1016/j.apcatb.2020.119648.
[18] Y. Wang, S. Kazumi, W. Gao, X. Gao, H. Li, X. Guo, Y. Yoneyama, G. Yang, N. Tsubakia, Direct conversion of CO_2 to aromatics with high yield via a modified Fischer-Tropsch synthesis pathway, Appl. Catal. B 269 (2020) 118792, https://doi.org/10.1016/j.apcatb.2020.118792.
[19] X. Cui, P. Gao, S. Li, C. Yang, Z. Liu, H. Wang, L. Zhong, Y. Sun, Selective production of aromatics directly from carbon dioxide hydrogenation, ACS Catal. 9 (2019) 3866–3876, https://doi.org/10.1021/acscatal.9b00640.
[20] C. Li, A. Vidal Moya, P. Miguel, J. Dedecek, M. Boronat, A. Corma, Selective introduction of acid sites in different confined positions in ZSM-5 and its catalytic implications, ACS Catal. 8 (2018) 7688–7697, https://doi.org/10.1021/acscatal.8b02112.
[21] T. Yokoi, H. Mochizuki, T. Biligetu, Y. Wang, T. Tatsumi, Unique Al distribution in the MFI framework and its impact on catalytic properties, Chem. Lett. 46 (2017) 798–800, https://doi.org/10.1246/cl.170156.
[22] J. Iorio, S. Li, C. Jones, C. Nimlos, Y. Wang, E. Kunkes, V. Vattipalli, S. Prasad, A. Moini, W. Schneider, R. Gounder, Cooperative and competitive occlusion of

organic and inorganic structure-directing agents within chabazite zeolites influences their aluminum arrangement, J. Am. Chem. Soc. 142 (2020) 4807–4819, https://doi.org/10.1021/jacs.9b13817.
[23] K. Muraoka, W. Chaikittisilp, Y. Yanaba, T. Yoshikawa, T. Okubo, Directing aluminum Atoms into energetically favorable tetrahedral sites in a zeolite framework by using organic structure-directing agents, Angew. Chem. Int. Ed. 57 (2018) 3742–3746, https://doi.org/10.1002/anie.201713308.
[24] X. Tang, Z. Liu, L. Huang, W. Chen, C. Li, G. Wang, G. Li, X. Yi, A. Zheng, Violation or abidance of lÖwensteins rule in zeolites under synthesis condition, ACS Catal. 9 (2019) 10618–10625, https://doi.org/10.1021/acscatal.9b01844.
[25] A. Rownaghi, J. Hedlund, Methanol to gasoline-range hydrocarbons: influence of nanocrystal size and mesoporosity on catalytic performance and product itribution of ZSM-5, Ind. Eng. Chem. 50 (2011) 11872–11878, https://doi.org/10.1021/ie201549j.
[26] T. Xue, L. Chen, Y. Wang, M. He, Seed-induced synthesis of mesoporous ZSM-5 aggregates using tetrapropylammonium hydroxide as single template, Microporous Mesoporous Mater. 156 (2012) 97–105, https://doi.org/10.1016/j.micromeso.2012.02.022.
[27] K. Na, M. Choi, W. Park, Y. Sakamoto, O. Terasaki, R. Ryoo, Pillared MFI zeolite nanosheets of a single-unit-cell thickness, J. Am. Chem. Soc. 132 (2010) 4169–4177, https://doi.org/10.1021/ja908382n.
[28] M. Choi, K. Na, J. Kim, Y. Sakamoto, O. Terasaki, R. Ryoo, Stable single-unit-cell nanosheets of zeolite MFI as active and long-lived catalysts, Nature 461 (2009) 246–249, https://doi.org/10.1038/nature08288.
[29] G. Kresse, J. Furthmiiller, Efficiency of ab-initio total energy calculations for metals and semiconductors using a plane-wave basis set, Comput. Mater. Sci. 6 (1996) 15–50, https://doi.org/10.1016/0927-0256(96)00008-0.
[30] G. Kresse, J. Furthmuller, Efficient iterative schemes for ab initio total-energy calculations using a plane-wave basis set, Phys. Rev. B. 54 (1996) 11169–11186, https://doi.org/10.1103/PhysRevB.54.11169.
[31] G. Kresse, J. Furthmiiller, From ultrasoft pseudopotentials to the projector augmented-method, Phys. Rev. B. 59 (1999) 1758–1775, https://doi.org/10.1103/PhysRevB.59.1758.
[32] J. Perdew, K. Burke, M. Ernzerhofof, Generalized gradient approximation made simple, Phys. Rev. Lett. 77 (1996) 3865–3868, https://doi.org/10.1103/PhysRevLett.77.3865.
[33] S. Grimme, J. Antony, S. Ehrlich, H. Krieg, J. Chem. Phys. A consistent and accurate ab initio parametrization of density functional dispersion correction (DFT-D) for the 94 elements H-Pu, 132 (2010) 154104-154119. https://doi.org/10.1063/1.3382344.
[34] H. Wang, Y. Hou, W. Sun, Q. Hu, H. Xiong, T. Wang, B. Yan, W. Qian, Insight into the effects of water on the ethene to aromatics reaction with HZSM-5, ACS Catal. 10 (2020) 5288–5298, https://doi.org/10.1021/acscatal.9b05552.
[35] G. Henkelman, H. Jónsson, Improved tangent estimate in the nudged elastic band method for finding minimum energy paths and saddle points, J. Chem. Phys. 113 (2000) 9978–9985, https://doi.org/10.1063/1.1323224.
[36] Y. Xu, P. Zhai, Y. Deng, J. Xie, X. Liu, S. Wang, D. Ma, Highly selective olefin production from CO_2 hydrogenation on iron catalysts: a subtle synergy between manganese and sodium additives, Angew. Chem. Int. Ed. 59 (2020) 21736–21744, https://doi.org/10.1002/anie.202009620.
[37] S. Wang, L. Zhang, S. Li, Z. Qin, D. Shi, S. He, K. Yuan, P. Wang, T. Zhao, S. Fan, M. Don, J. Li, W. Fan, J. Wang, Tuning the siting of aluminum in ZSM-11 zeolite and regulating its catalytic performance in the conversion of methanol to olefins, J. Catal. 377 (2019) 81–97, https://doi.org/10.1016/j.jcat.2019.07.028.
[38] T. Liang, J. Chen, Z. Qin, J. Li, P. Wang, S. Wang, G. Wang, M. Dong, W. Fan, J. Wang, Conversion of methanol to olefins over H-ZSM-5 zeolites: Reaction pathway is related to the framework aluminum siting, ACS Catal. 6 (2016) 7311–7325, https://doi.org/10.1021/acscatal.6b01771.
[39] T. Biligetu, Y. Wang, T. Nishitoba, R. Otomo, S. Park, H. Mochizuki, J. Kondo, T. Tatsumi, T. Yokoi, Al distribution and catalytic performance of ZSM-5 zeolites synthesized with various alcohols, J. Catal. 353 (2017) 1–10, https://doi.org/10.1016/j.jcat.2017.06.026.
[40] Y. Wang, X. Liu, X. He, F. Yang, X. Zhu, Tailoring the framework aluminum arrangement in ZSM-5 zeolites to regulate reaction route for alkylation of benzene with methanol, Microporous Mesoporous Mater. 351 (2023) 112491, https://doi.org/10.1016/j.micromeso.2023.112491.
[41] J. Dědeček, S. Sklenak, C. Li, B. Wichterlová, V. Gábová, J. Brus, M. Sierka, J. Sauer, Effect of Al-Si-Al and Al-Si-Si-Al pairs in the ZSM-5 zeolite framework on the ^{27}Al NMR spectra. A combined high-resolution ^{27}Al NMR and DFT/MM study, J. Phys. Chem. C. 113 (2009) 1447–1458, https://doi.org/10.1021/jp8068333.
[42] S. Sklenak, J. Dědeček, C. Li, B. Wichterlová, V. Gábová, M. Sierka, J. Sauer, Aluminum siting in silicon-rich zeolite frameworks: a combined high-resolution 27 Al NMR spectroscopy and quantum mechanics/molecular mechanics study of ZSM-5, Angew. Chem. Int. Ed. 46 (2007) 7286–7289, https://doi.org/10.1002/anie.200702628.
[43] S. Wang, P. Wang, Z. Qin, Y. Chen, M. Dong, J. Li, K. Zhang, P. Liu, J. Wang, W. Fan, Relation of catalytic performance to the aluminum siting of acidic zeolites in the conversion of methanol to olefins, viewed via a comparision between ZSM-5 and ZSM-11, ACS Catal. 8 (2018) 5485–5505, https://doi.org/10.1021/acscatal.8b01054.
[44] S. Xin, Q. Wang, J. Xu, Y. Chu, P. Wang, N. Feng, G. Qi, J. Trébosc, O. Lafon, W. Fan, F. Deng, The acidic nature of "NMR-invisible" tri-coordinated framework aluminum species in zeolites, Chem. Sci. 10 (2019) 10159–10169, https://doi.org/10.1039/C9SC02634G.
[45] X. Niu, J. Gao, Q. Miao, M. Dong, G. Wang, W. Fan, Z. Qin, J. Wang, Influence of preparation method on the performance of Zn-containing HZSM-5 catalysts in methabol-to-aromatics, Microporous Mesoporous Mater. 197 (2014) 252–261, https://doi.org/10.1016/j.micromeso.2014.06.027.
[46] Y. Joshi, A. Bhan, K. Thomson, DFT-based reaction pathway analysis of hexadiene cyclization via carbenium ion intermediates: Mechanistic study of light alkane aromatization catalysis, J. Phys. Chem. B 108 (2004) 971–980, https://doi.org/10.1021/jp036205m.
[47] Y. Wongnongwa, P. Kidkhunthod, U. Sukkha, S. Pengpanich, K. Thavornprasert, J. Phupanit, N. Kungwan, G. Feng, T. Keawin, S. Jungsuttiwong, Local structure elucidation and reaction mechanism of light naphtha aromatization over Ga embedded H-ZSM-5 zeolite: combined DFT and experimental study, Microporous Mesoporous Mater. 306 (2020) 110414, https://doi.org/10.1016/j.micromeso.2020.110414.
[48] S. Bailleul, I. Yarulina, A.E.J. Hoffman, A. Dokania, E. Abou-Hamad, A. D. Chowdhury, G. Pieters, J. Hajek, K.D. Wispelaere, M. Waroquier, J. Gascon, V. V. Speybroeck, A supramolecular view on the cooperative role of bronsted and lewis acid sites in zeolites for methanol conversion, J. Am. Chem. Soc. 141 (2019) 14823–14842, https://doi.org/10.1021/jacs.9b07484.
[49] C. Hsieh, Y. Chen, Y. Lin, Ga-substituted nanoscale HZSM-5 in methanol aromatization: The cooperative action of the Brønsted acid and the extra-framework Ga species, Ind. Eng. Chem. Res. 57 (2018) 7742–7751, https://doi.org/10.1021/acs.iecr.8b00126.
[50] P. Gao, J. Xu, G. Qi, C. Wang, Q. Wang, Y. Zhao, Y. Zhang, N. Feng, X. Zhao, J. Li, F. Deng, A mechanistic study of methanol-to-aromatics reaction over Ga-modified ZSM-5 zeolites: understanding the dehydrogenation process, ACS Catal. 8 (2018) 9809–9820, https://doi.org/10.1021/acscatal.8b03076.
[51] S. Müller, Y. Liu, F. Kirchberger, M. Tonigold, M. Sanchez-Sanchez, J. Lercher, Hydrogen transfer pathways during zeolite catalyzed methanol conversion to hydrocarbons, J. Am. Chem. Soc. 138 (2016) 15994–16003, https://doi.org/10.1021/jacs.6b09605.
[52] W. Wang, C. Liu, W. Wu, Bifunctional catalysts for the hydroisomerization of n-alkenes: the effects of metal-acid balance and textural structure, Catal. Sci. Technol. 9 (2019) 4162–4187, https://doi.org/10.1039/C9CY00499H.
[53] M. He, J. Zhang, R. Liu, X. Sun, B. Chen, Y. Wang, Density functional theory studies on the skeletal isomerization of 1-butene catalyzed by HZSM-23 and HZSM-48 zeolites, RSC Adv. 7 (2017) 9251–9257, https://doi.org/10.1039/C6RA26894C.
[54] M. Boronat, P. Viruelab, A. Corma, The skeletal isomerization of but-1-ene catalyzed by theta-1 zeolite, Phys. Chem. Chem. Phys. 3 (2001) 3235–3239, https://doi.org/10.1039/B103429B.
[55] M. Boronat, P. Viruela, A. Corma, Theoretical study of the mechanism of zeolite-catalyzed isomerization reactions of linear butenes, J. Phys. Chem. A 102 (1998) 982–989, https://doi.org/10.1021/jp972672q.
[56] J. Wei, R. Yao, Q. Ge, Z. Wen, X. Ji, C. Fang, J. Zhang, H. Xu, J. Sun, Catalytic hydrogenation of CO_2 to isoparaffins over Fe-based multifunctional catalysts, ACS Catal. 8 (2018) 9958–9967, https://doi.org/10.1021/acscatal.8b02267.
[57] Y. Peng, X. Wang, C. Wang, W. Bi, Q. Jiang, Z. Tian, Boosting catalytic performance via electron transfer effect for hydroisomerization on a low-Pt-content PtCeOx/zeolite catalyst, Chem. Catal. 3 (2023) 100505, https://doi.org/10.1016/j.checat.2023.100505.